Mon. Not. R. Astron. Soc. **000**, 1–16 (2013) Printed 21 January 2014 (MN LATEX style file v2.2)

Hydrodynamical simulations of coupled and uncoupled quintessence models I: Halo properties and the cosmic web

Edoardo Carlesi,[1] ⋆ Alexander Knebe,[1] Geraint F. Lewis,[2] Scott Wales,[2,3] Gustavo Yepes[1]
[1]*Departamento de Física Teórica, Universidad Autónoma de Madrid, 28049, Cantoblanco, Madrid, Spain*
[2]*Sydney Institute for Astronomy, School of Physics, A28, The University of Sydney, NSW 2006, Australia*
[3]*ARC Centre of Excellence for Climate System Science, School of Earth Sciences, The University of Melbourne, Australia 3010*

arXiv:1401.5005v1 [astro-ph.CO] 20 Jan 2014

Accepted XXXX . Received XXXX; in original form XXXX

ABSTRACT

We present the results of a series of adiabatic hydrodynamical simulations of several quintessence models (both with a free and an interacting scalar field) in comparison to a standard ΛCDM cosmology. For each we use 2×1024^3 particles in a $250h^{-1}\,\mathrm{Mpc}$ periodic box assuming WMAP7 cosmology. In this work we focus on the properties of haloes in the cosmic web at $z = 0$. The web is classified into *voids*, *sheets*, *filaments* and *knots* depending on the eigenvalues of the velocity shear tensor, which are an excellent proxy for the underlying overdensity distribution. We find that the properties of objects classified according to their surrounding environment shows a substantial dependence on the underlying cosmology; for example, while V_{max} shows average deviations of ≈ 5 per cent across the different models when considering the full halo sample, comparing objects classified according to their environment, the size of the deviation can be as large as 20 per cent.

We also find that halo spin parameters are positively correlated to the coupling, whereas halo concentrations show the opposite behaviour. Furthermore, when studying the concentration-mass relation in different environments, we find that in all cosmologies underdense regions have a larger normalization and a shallower slope. While this behaviour is found to characterize all the models, differences in the best-fit relations are enhanced in (coupled) dark energy models, thus providing a clearer prediction for this class of models.

Key words: methods:N-body simulations – galaxies: haloes – cosmology: theory – dark matter

1 INTRODUCTION

Over more than 15 years, since observations of high-redshift Supernovae of type Ia (see Riess et al. 1998; Perlmutter et al. 1999) first indicated that the Universe is undergoing an accelerated expansion, a large number of cosmological probes, including cosmic microwave background (CMB) anisotropies (Larson et al. 2011; Sherwin et al. 2011), weak lensing (Huterer 2010), baryon acoustic oscillations (BAO) (Beutler et al. 2011) and large scale structure (LSS) surveys (Abazajian et al. 2009), have confirmed this startling claim and shown that the Universe is spatially flat. To explain these diverse observation, cosmology requires the presence of a fluid, called dark energy (DE), which permeates the whole Universe and exerts a negative pressure, eventually overcoming the gravitational pull that would otherwise dominate. The standard model of cosmology, referred to as ΛCDM, provides the simplest possible explanation for DE, assuming that DE is played by a constant called Λ which possesses a constant equation of state, such that $p_\Lambda = -\rho_\Lambda$. However, despite its simplicity and observational viability, ΛCDM still lacks of appeal from a purely theoretical point of view, due to *fine tuning* and *coincidence* problems; the first refers to the fact that, if we assume that Λ is the zero-point energy of a fundamental quantum field, to be compatible with the aforementioned cosmological constraints its density requires an unnatural fine-tuning of several tens of orders of magnitude. The second problem arises from the difficulty in explaining in a satisfactory way the fact that matter and dark energy densities *today* have comparable values, although throughout most of the cosmic history their evolutions have followed completely different patterns.

It is thus natural to explore the possibility that dark energy does not take the form of a cosmological constant, Λ, but is instead a dynamical component of the universe, whose energy density evolves with time, eventually dominating in the present epoch. In this sense, a large number of different models, such as Chaplygin gas (Kamenshchik et al. 2001), vector dark energy (Beltrán Jiménez & Maroto 2008; Carlesi et al. 2012), κ-essence (Armendariz-Picon et al. 2000) and quintessence (Wetterich 1995; Caldwell et al. 1998; Copeland et al. 1998; Zlatev et al. 1999) have been proposed to overcome the perceived theoretical shortcomings of the standard cosmology. In particular, quintessence (or scalar

⋆ E-mail: edoardo.carlesi@uam.es

© 2013 RAS

field) models are viable and likely candidates for dynamical dark energy (see Tsujikawa 2013), as they can reproduce current observational data without being plagued by the fine-tuning problem of ΛCDM, since their expansion history - at least for a set of different potentials - is almost insensitive to the particular choice of the field's initial conditions. An interesting subset of quintessence theories is represented by coupled models, where it is assumed that the scalar field has a non-negligible interaction to the dark matter sector (Amendola 2000) and is thus expected to leave a strong imprint on structure formation.

While both classes of quintessence models have been already studied numerically by means of N-body simulations (see for instance Klypin et al. (2003), De Boni et al. (2011) for free and Baldi et al. (2010), Li & Barrow (2011b) for coupled models), in the present work we aim at investigating and highlighting the differences arising among coupled and uncoupled scalar fields with the same potential, and compare our results to a benchmark ΛCDM cosmology. Our aim is to disentangle the effects due to the *fifth force* acting on dark matter particles from those caused to the dynamical nature of dark energy, when considering the deeply non-linear regime of the models. This way we will discern strategies to observationally distinguish between coupled and uncoupled forms of quintessence and thus to provide new tools for model selection.

Using a suitably modified version of the publicly available SPH/N-body code GADGET-2 (Springel 2005) we undertake a series of simulations of different quintessence models with a Ratra-Peebles (Ratra & Peebles 1988) potential and several values of the coupling parameter allowed by current observational constraints. The box size ($250h^{-1}\,\mathrm{Mpc}$), the number of particles (2×1024^3) and the use of adiabatic smoothed particle hydrodynamics allow us to analyse a large amount of different properties with a good resolution and statistics. In this first of a series of papers, we will consider large-scale structures (LSS) and its environment, with the physics of galaxy clusters presented in a follow-up paper (Paper II). In the present work, we analyze in particular the structure of the cosmic web and the correlations between the environment, dark matter haloes and gas across these different cosmological models.

The paper is organized as follows; in Section 2, we briefly recall the general features of the quintessence models considered in this work as well as of the recipes necessary for their simulation using N-body techniques. In Section 3, we discuss the settings of our particular simulations as well as those of the halo finder, together with the classification of the cosmic web. In Section 4 we present LSS properties of the modified frameworks, Section 5 is dedicated to the general features of the cosmic web while in Section 6 we describe the results of the correlation of haloes to their environment. A summary of the results obtained and a discussion on their implications is then presented in section Section 7.

2 PREREQUISITES

Here, we will briefly recall the basic properties of quintessence models and their implementation into a cosmological N-body algorithm. We refer the reader to the works of Wetterich (1995); Amendola (2000); Amendola & Quercellini (2003); Pettorino et al. (2012); Chiba et al. (2013) for discussions on the theoretical and observational properties of (coupled) quintessence models, and to Macciò et al. (2004); Baldi et al. (2010); Li & Barrow (2011a) for a thorough description of the numerical approaches.

Table 1. Values of the coupling and potential used for the uDEand cDE models.

Model	V_0	α	β
uDE	10^{-7}	0.143	–
cDE033	10^{-7}	0.143	0.033
cDE066	10^{-7}	0.143	0.066
cDE099	10^{-7}	0.143	0.099

2.1 The models

In quintessence models the role of dark energy is played by a cosmological scalar field ϕ whose Lagrangian can be generally written as:

$$L = \int d^4x\sqrt{-g}\left(-\frac{1}{2}\partial_\mu\partial^\mu\phi + V(\phi) + m(\phi)\psi_m\bar{\psi}_m\right) \quad (1)$$

where in principle ϕ can interact with the dark matter field ψ_m through its mass term, meaning that, in general, dark matter particles will have a time-varying mass. With a suitable choice of the potential $V(\phi)$, quintessence cosmologies can account for the late time accelerated expansion of the universe both in the interacting and non interacting case. In the present work we have focused on the so called Ratra-Peebles (see Ratra & Peebles 1988) self interaction potential:

$$V(\phi) = V_0\left(\frac{\phi}{M_p}\right)^{-\alpha} \quad (2)$$

where M_p is the Planck mass, while V_0 and α are two constants whose values can be fixed by fitting the model to observational data (see Wang et al. 2012; Chiba et al. 2013).

In Eq. (1), we allowed for the scalar field to interact with matter through the mass term $m(\phi)\psi\bar{\psi}$; a popular choice (Pettorino et al. 2012, see) for the function $m(\phi)$ is:

$$m(\phi) = m_0\exp\left(-\beta(\phi)\frac{\phi}{M_p}\right) \quad (3)$$

which is also the one assumed in this *paper*.

In the following, we have taken into account a constant interaction term $\beta(\phi) = \beta_0$, which from Eq. (3) implies an energy flow from the dark matter to the dark energy sector and thus a diminishing mass for dark matter particles. In Table 1 we list the values for V_0, α and β of Eq. (2) and Eq. (3) as used in the four non-standard cosmologies under investigation - an uncoupled Dark Energy (uDE) model and three coupled Dark Energy (cDE) ones. The latter differ only by the choice of the coupling and have been named accordingly. The particular values used in all the implementations have been selected according to the Cosmic Microwave Background (CMB) constraints discussed in Pettorino et al. (2012), to ensure the cosmologies under investigation to be compatible with the WMAP7 dataset (Komatsu et al. 2011). However, more recent results obtained using Planck data (see Pettorino 2013), provide even tighter constraints on the free parameters of these models, which shall be the object of subsequent investigation.

2.2 Numerical implementation

The first simulations of interacting dark energy models were performed by Macciò et al. (2004), who described the basic steps for implementing interacting quintessence into the ART code. In our

Table 2. Cosmological parameters at $z = 0$ used in the ΛCDM, uDE, cDE033, cDE066 and cDE099 simulations.

Parameter	Value
h	0.7
n	0.951
Ω_{dm}	0.224
Ω_b	0.046
σ_8	0.8

case, we built our implementation on `P-GADGET2`, a modified version of the publicly available code `GADGET2` (Springel et al. 2001; Springel 2005). This version has first been developed to simulate vector dark energy models (see Carlesi et al. 2011, 2012) and was then extended to generic dynamical dark energy as well as coupled dark energy cosmologies. The algorithm used is based on the standard Tree-PM solver with some modifications added to take into account the additional long-range interactions due to the coupled scalar field which effectively act as a rescaling of the gravitational constant. For the implementation of these features non-standard models we followed closely the recipe described in Baldi et al. (2010), to which the reader is referred.

This approach requires that a number of quantities, namely:

- the full evolution of the scalar field ϕ and its derivative $\dot{\phi}$,
- the variation mass of cold dark matter particles $\Delta m(z)$, and
- the background expansion $H(z)$.

have to be computed in advance and then interpolated at run time. We therefore implemented background and first order Newtonian perturbation equations into the publicly available Boltzmann code `CMBEASY` (Doran 2005) to generate the tables containing the aforementioned quantities. The starting background densities were chosen in order to ensure the same values at $z = 0$ for the cosmological parameters listed in Table 2; linear perturbations have been solved assuming adiabatic initial conditions.

Finally, in the case of non-standard cosmologies it is necessary to properly generate the initial conditions of the N-body simulations taking into account not only the different matter power spectra but also the altered growth factors and logarithmic growth rates, respectively. These are in fact the necessary ingredients to compute the initial particles' displacements and velocities on a uniform Cartesian grid using the first order Zel'dovich approximation (Zel'dovich 1970). We implemented these changes into the publicly available `N-Genic`[1] MPI code, which is suitable for generating `GADGET` format initial conditions. Again, the matter power spectra, growth factors $D(t)$ and logarithmic growth rates $f = d\ln D(t)/d\ln a$ have been computed for the four non-standard cosmologies using the modified `CMBEASY` package.

All the above changes have been carefully tested against theoretical predictions and the previous results existing in the literature to ensure the consistency and reliability of our modifications.

Table 3. N-body settings and cosmological parameters used for the three simulations.

Parameter	Value
L_{box}	$250h^{-1}\,\mathrm{Mpc}$
N_{dm}	1024^3
N_{gas}	1024^3
m_{dm}	$9.04 \times 10^8 h^{-1}\mathrm{M}_\odot$
m_b	$1.85 \times 10^8 h^{-1}\mathrm{M}_\odot$
z_{start}	60

3 THE SIMULATIONS

3.1 Settings

Our set of N-body simulation has been devised in order to allow us to compare and quantitatively study the peculiarities of the different models in the physics of galaxy clusters and the properties of the cosmic web. To do this, we have chosen a box of side length $250h^{-1}\,\mathrm{Mpc}$ (comoving) where we expect to be able to analyze with adequate resolution a statistically significant (> 100) number of galaxy clusters ($M > 10^{14}h^{-1}\mathrm{M}_\odot$) as well as the properties of the different cosmic environments, classified as voids, sheets, filaments and knots. The parameters chosen to set up the simulations, which are common to all the six models under investigation, are listed in Table 3.

In this series of simulations we implemented adiabatic SPH only, thus neglecting the effects of all sources of radiative effects (Monaghan 1992; Springel 2010) This way we are able to establish a clear basis for the differences induced on baryons by the different cosmologies, without the need to take into account the additional layer of complexity introduced of radiative physics, which in itself requires a substantial degree of modeling. The publicly available version of `GADGET-2` performs a Lagrangian sampling of the continuous fluid quantities using a set of discrete tracer particles. Gas dynamics equations are then solved using the SPH entropy conservation scheme described in Springel (2005). In our case, continuous fluid quantities are computed using a number of smoothing neighbours $N_{sph} = 40$. Gas pressure and density are related through the relation $P \propto \rho^\gamma$, where $\gamma = \frac{5}{3}$ under the adiabatic assumption.

In addition to the four quintessence models (whose parameters have been given in Table 1) we simulated a ΛCDM cosmology, which we use as a benchmark to pinpoint deviations from the standard paradigm. The initial conditions for all the simulations have been generated using the same random phase realization for the Gaussian fluctuations, which enables us to consistently cross-correlate properties enforcing the same values at present time for Ω_m and σ_8 (cf. Table 2), across different simulations.

3.2 Halo identification

We identified haloes in our simulation using the open source halo finder `AHF`[2] described in Knollmann & Knebe (2009); this code improves the `MHF` halo finder (Gill et al. 2004) and has been widely compared to a large number of alternative halo finding methods (Knebe et al. 2011; Onions et al. 2012; Knebe et al. 2013). `AHF` computes the density field and locates the prospective halo centres

[1] http://www.mpa-garching.mpg.de/gadget/

[2] `AHF` stands for Amiga Halo Finder, which can be downloaded freely from `http://www.popia.ft.uam.es/AHF`

at the local overdensities. For each of these density peaks, it determines the gravitationally bound particles, retaining only peaks with at least 20 of them, which are then considered as haloes and further analyzed.

The mass is computed via the equation

$$M_\Delta = \Delta \times \rho_c(z) \times \frac{4\pi}{3} R_\Delta^3. \quad (4)$$

so that $M(R)$ is defined as the total mass contained within a radius R at which the halo matter overdensity reaches Δ times the critical value ρ_c. Since the critical density of the universe is a function of redshift, we must be careful when considering its definition, which reads

$$\rho_c(z) = \frac{3H^2(z)}{8\pi G} \quad (5)$$

as the evolution of the Hubble parameter, $H(z)$ differs at all redshifts in the five models. In the latest version of AHF this problem is solved reading the $H(z)$ for the cDE and uDE models in from a precomputed table, which then allows to compute the $\rho_c(z)$ consistently in each case. For all models we assume $\Delta = 200$.

3.3 Classification of the cosmic web

As we intend to correlate halo properties with the environment, it is necessary to introduce the algorithm used for the classification of the cosmic web into voids, sheets, filaments and knots. Using the term cosmic web (Bond et al. 1996) we refer to the complex visual appearance of the large scale structure of the universe, characterized by thin linear filaments and compact knots crossing regions of very low density (Massey et al. 2007; Kitaura et al. 2009; Jasche et al. 2010).

The exact mathematical formulation for describing the visual impression of the web is highly non-trivial and can be implemented using two different approaches, the geometric one and the dynamic one. The first one relies on the spatial distribution of haloes in simulations (Novikov et al. 2006; Aragón-Calvo et al. 2007) disregarding the dynamical context. The second approach starts with the classification of Hahn et al. (2007), where they identified the type of environment using the eigenvalues of the tidal tensor (i.e. the Hessian of the gravitational potential), rather than studying the matter density distribution.

However, these particular approaches are unable to resolve the web on scales smaller than a few megaparsecs (Forero-Romero et al. 2009). While retaining the original idea of dynamical classification, Hoffman et al. (2012) proposed to replace the tidal tensor with the velocity shear, showing that this approach has a much finer resolution on the smaller scales while reproducing the large scale results of the other approach. Defining the velocity shear tensor as

$$\Sigma_{\alpha\beta} = -\frac{1}{2H_0}\left(\frac{\partial v_\alpha}{\partial r_\beta} - \frac{\partial v_\beta}{\partial r_\alpha}\right) \quad (6)$$

and diagonalizing it, we obtain the eigenvalues λ_1, λ_2 and λ_3. Taking the trace of $\Sigma_{\alpha\beta}$ we obtain

$$Tr(\Sigma_{\alpha\beta}) = \sum_i \lambda_i = -\overrightarrow{\nabla} \cdot \overrightarrow{V} \propto \delta_m \quad (7)$$

from which we see that there is indeed a direct relationship between the eigenvalues of the velocity shear tensor and the matter overdensity. In practice the eigenvalue λ_i is related to the intensity of the inflow (outflow) of matter along the i-th axis in the base where $\Sigma_{\alpha\beta}$ is diagonal.

We therefore proceed to classify the cosmic web ordering the eigenvalues $\lambda_1 > \lambda_2 > \lambda_3$ and defining the different points on the web as (Hoffman et al. 2012; Libeskind et al. 2012, 2013):

- *voids*, if $\lambda_1 < \lambda_{th}$
- *sheets*, if $\lambda_1 > \lambda_{th} > \lambda_2$
- *filaments*, if $\lambda_2 > \lambda_{th} > \lambda_3$
- *knots*, if $\lambda_3 > \lambda_{th}$

where λ_{th} is a free threshold parameter (to be specified below).

The computation of the eigenvalues has been performed on a regular 256^3 grid, corresponding to a cell size of $0.97h^{-1}\,\mathrm{Mpc}$. We use a triangular-shaped cloud (TSC) prescription for the assignment of the particles (Hockney & Eastwood 1988) and then compute the overdensity and the eigenvalues of the velocity shear tensor for every grid cell. Using the AHF catalogues, we assign every halo to the nearest grid point hence providing us with a measure of environment for every object.

At this stage we still have not explicitly classified the cosmic web, as we lack a clear theoretical prescription for the value of λ_{th}. In our case, we have fixed λ_{th} to the highest value which ensures that no halo with $M > 10^{14}h^{-1}\mathrm{M}_\odot$ belongs to a void in any simulation. At a first glance, this kind of constraint might seem redundant, as it would be implied in any standard definition of void as an underdense region. However, we must recall here that our definition of the cosmic web relies solely on the dynamical properties of the matter distribution (being related to the magnitude of its inflow or outflow in a given node) and may in principle overlook its net density content. It is thus necessary to enforce this principle explicitly tuning our free parameter to $\lambda_{th} = 0.1$, which is the value which in this case satisfies the aforementioned condition and has been used in Section 5. For a more elaborate discussion of λ_{th} we refer the reader to Hoffman et al. (2012); we only note that our choice is close to their proposed value.

4 LARGE SCALE CLUSTERING AND GENERAL PROPERTIES

Before presenting the results relative to the properties of the cosmic web and the correlation of halo properties to the environment, we will describe some aspects of large scale structure (LSS) and general halo properties in our simulations. This should give a more traditional overview of the effects of (coupled) dark energy models.

4.1 Halo mass function

The halo mass function (HMF) in coupled dark energy cosmologies has already been studied by Macciò et al. (2004); Nusser et al. (2005); Baldi et al. (2010); Li & Barrow (2011b); Cui et al. (2012) so that we will only briefly comment on the topic. Our results reproduce the earlier findings of Baldi's in the overlapping regions of mass and k-space, thus providing an additional proof of the correct functioning of our modified implementation.

In Fig. 1 we show the cumulative mass (left) and velocity functions (right) as well as the ratio to ΛCDM for the four quintessence models. Singling out the region from 10^{10} to $10^{14}\ h^{-1}\mathrm{M}_\odot$, and neglecting the higher mass end, where the statistics is unreliable due to the low number of objects, we can see that the largest difference in number counts amounts to $\approx 7\%$ for the strongest coupled

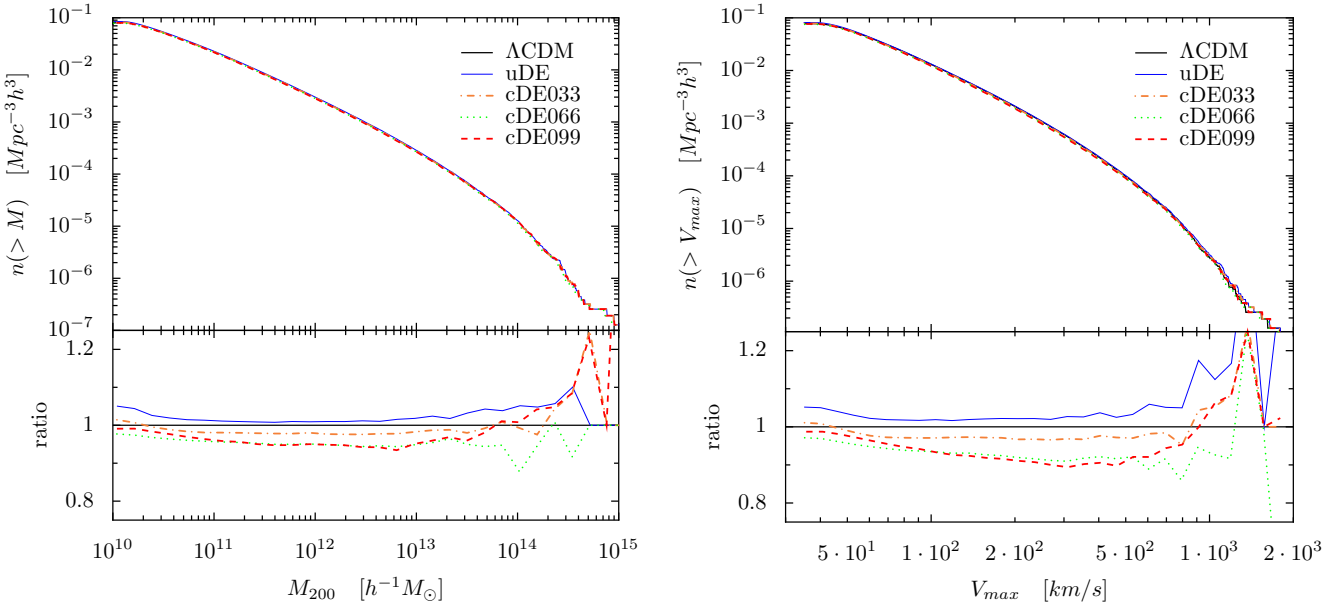

Figure 1. Cumulative halo density number counts as a function of mass (left panel) and V_{max} (right panel). Compared to ΛCDM, a slight suppression of the number of objects produced at redshift $z = 0$ is predicted for cDE models while the opposite is true for uDE. Albeit small, the effect is enhanced in the velocity function, where the strongest coupled model differs up to 10% from ΛCDM (neglecting the higher mass ends, which are affected by a very low statistics).

models, gradually decreasing for smaller couplings. In the velocity function, this suppression reaches 10%, thus slightly enhancing the magnitude of the effect.

We can compare our results for the HMF with those of Cui et al. (2012), who modeled the Jenkins et al. (2001) and Tinker et al. (2008) mass functions for a series of similar coupled dark energy models, using Friends-of-Friends (FoF) and Spherical Overdensity (SO) algorithms to build up their halo catalogues. Even though in their simulations they used different σ_8 normalizations, fitting the analytical HMFs to the numerical results they were able to extend the predictions for cDE cosmology to arbitrary σ_8 values. Using the same ΛCDM σ_8 normalization, then, they also found a $5-10\%$ suppression of the HMF of cDE, in perfect agreement with our results.

Although not shown here, we have also verified that these $z = 0$ results match the analytical prediction of the Tinker mass function (Tinker et al. 2008), provided the correct input power spectra and normalizations are used. We can safely conclude that the presence of coupled and uncoupled quintessence of the kind described here is expected to produce differences from ΛCDM predictions up to a factor 10% in present day's HMF. Remarkably, this estimate is qualitatively independent of the algorithm used for the halo identification as we have seen comparing our results to the work of Cui et al. (2012).

4.2 Halo properties

To study internal halo properties (such as spin parameter and concentration) we first need to define a statistically sound sample of objects, in order to reduce the impact of spurious effects on the results. This means that we need to constrain our analysis to structures which satisfy some conditions on both *resolution* and *relaxation*.

The first condition means that we have to restrict our analysis to objects with a number of particles above a given threshold, taking into account the existing trade-off between the quality and the size of the halo sample. The second criterion needs to be applied as we want to focus on structures as close as possible to a state of dynamical equilibrium. In fact, many phenomena, such as infalling matter and major mergers, may take place, driving the structure out of equilibrium. In this case, then, the determination of quantities such as density profiles and concentrations becomes unreliable (see for instance Macciò et al. (2007) and Muñoz-Cuartas et al. (2011)).

Following Prada et al. (2012), we will define as relaxed only the haloes that obey to the condition

$$\frac{2K}{|U|} - 1 < 0.5 \tag{8}$$

without introducing other selection parameters; for alternative ways of identifying unrelaxed objects we refer for instance to Macciò et al. (2007); Bett et al. (2007); Neto et al. (2007); Knebe & Power (2008); Prada et al. (2012); Muñoz-Cuartas et al. (2011); Power et al. (2012). For the moment, we neglect the impact of uDE and cDE on the definition of the virial ratio since this effect is of just a few percent (Abdalla et al. 2010; Pace et al. 2010) and is thus subleading in our case, where we are removing objects off by more than 50% from the standard relation.

Now that we have established the rules that will shape our halo sample, we proceed to study some internal properties of dark matter haloes, namely, spin and concentration – as a function of halo mass – enforcing one additional criterion for the halo selection: the number of particles in it. When studying the spin parameter, we will restrict ourselves to haloes with $M_{200} > 3 \times 10^{11} h^{-1}\mathrm{M}_\odot$, i.e. composed of at least ≈ 600 baryon and dark matter particles, following the choices of Bett et al. (2007), Macciò et al. (2007), Muñoz-Cuartas et al. (2011) and Prada et al. (2012). In the case of halo concentrations, we applied a stricter criterion, using $M_{200} > 1 \times 10^{12} h^{-1}\mathrm{M}_\odot$(or ≈ 2000 particles), due to the fact that the com-

Table 4. Total number of haloes found in each simulation corresponding to our applied mass cuts of $M > 3 \times 10^{11} h^{-1}\mathrm{M}_{\odot}$ and the $M > 10^{12} h^{-1}\mathrm{M}_{\odot}$, respectively.

Mass cut	ΛCDM	uDE	cDE033	cDE066	cDE099
$M > 3 \times 10^{11} h^{-1}\mathrm{M}_{\odot}$	138211	139288	135613	130877	130812
$M > 10^{12} h^{-1}\mathrm{M}_{\odot}$	46196	46179	44943	44363	43749

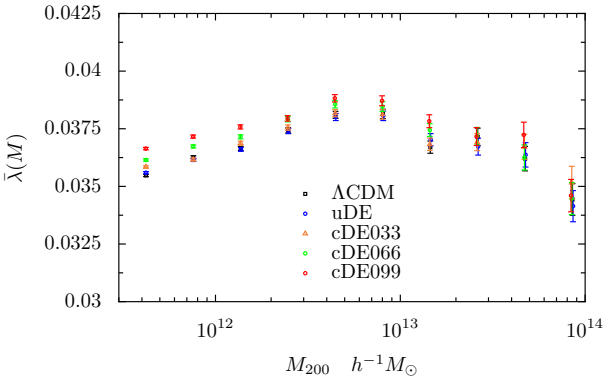

Figure 2. Average value of the spin parameter per mass bin. We can see that the spin parameter has a weak positive correlation to the mass until $\approx 8 \times 10^{12} h^{-1}\mathrm{M}_{\odot}$and a negative one after that threshold. Further, haloes in coupled dark energy models have an average value which is slightly larger than uncoupled ones.

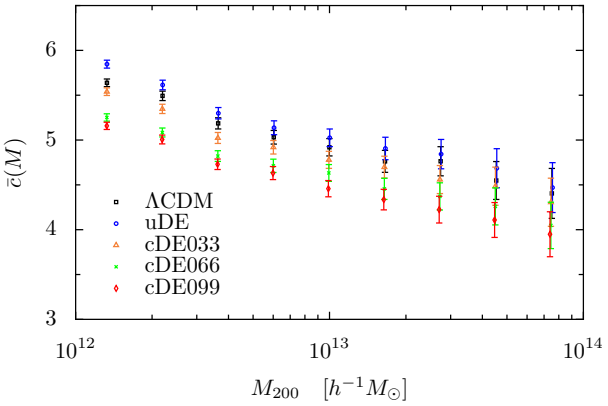

Figure 3. Halo mass concentration relation at $z = 0$, where the median concentration per mass bin is plotted. Compared to ΛCDM, cDE cosmologies show a systematically lower value of c for all mass bins, whereas for uDE it is larger.

putation of halo concentration requires a better resolution of the central regions, as we will discuss in the dedicated subsection.

4.2.1 *Spin parameter*

We can study the rotational properties of haloes introducing the so-called spin parameter λ (e.g. Barnes & Efstathiou 1987; Warren et al. 1992), a dimensionless number that measures the degree of rotational support of the halo. Following Bullock et al. (2001), we define it as

$$\lambda = \frac{L_{200}}{\sqrt{2} M_{200} V_{200} R_{200}} \tag{9}$$

where the quantities the total angular momentum L, the total mass M, the circular velocity V, and the radius R are all taken as defined by Eq. (4), with $\Delta = 200$; in cosmological simulations, the distribution of this parameter is found to be described as lognormal (e.g. Barnes & Efstathiou 1987; Warren et al. 1992; Cole & Lacey 1996; Gardner 2001; Bullock et al. 2001; Macciò et al. 2007, 2008; Muñoz-Cuartas et al. 2011)

$$P(\lambda) = \frac{1}{\lambda \sigma_0^2 \sqrt{2\pi}} \exp\left[-\frac{\ln^2(\lambda/\lambda_0)}{2\sigma_0^2} \right] , \tag{10}$$

even though some authors (e.g. Bett et al. 2007) claim that this should be slightly modified.

Due to the non-Gaussian nature of this distribution, instead of the average value we plot in Fig. 2 the median value of the spin parameter λ as a function of halo mass. A weak negative correlation of spin to the halo mass can be observed here for haloes above $8 \times 10^{12} h^{-1}\mathrm{M}_{\odot}$, (as noted for instance by Macciò et al. (2007) and Knebe & Power (2011)) while the relation is positive below that threshold. However, cDE models have on average a higher value (per mass bin) compared to uDE and ΛCDM. Albeit small, this increase in λ is clearly a coupling related effect, the magnitude of which is directly proportional to the value of β. Given the small error bars (due to the large number of objects used in this analysis) we are confident that this is a real effect. Moreover, a similar result has been found by Hellwing et al. (2011), that also claimed to have observed a link between fifth force and larger λs.

A deeper investigation of the physical link between the coupling and increased rotational support is left to an upcoming work (Carlesi et al., in prep.) where the *evolution* of different parameters under different cosmologies will be analyzed. For the moment it is important to note that there appears to be some evidence of a link between the coupling strength of the fifth force and the corresponding degree of rotational support in dark matter haloes.

4.2.2 *Concentration*

Dark matter density profiles can be described by a Navarro-Frenk-White (NFW) profile (Navarro et al. 1996), of the form

$$\rho(r) = \frac{\rho_0}{\frac{r}{r_s}\left(1 + \frac{r}{r_s}\right)^2} \tag{11}$$

where the r_s, the so called scale radius, and the density ρ_0 are in principle two free parameters that depend on the particular halo structure. Using Eq. (11) we can define

$$c = \frac{r_{200}}{r_s} \tag{12}$$

which is the *concentration* of the halo, relating the radius r_{200} to the scale radius r_s. Fitting Eq. (11) to our halo sample we observe that no substantial difference can be seen in the different simulations, that is, the NFW formula describes (on average) equally

Table 5. Best fit values for the mass concentration relation for haloes with $M > 10^{12}h^{-1}\mathrm{M}_{\odot}$.

Model	ΛCDM	uDE	cDE033	cDE066	cDE099
c_0	4.31 ± 0.06	4.48 ± 0.07	4.18 ± 0.06	3.98 ± 0.08	3.86 ± 0.06
γ	-0.088 ± 0.007	-0.093 ± 0.009	-0.083 ± 0.009	-0.084 ± 0.009	-0.079 ± 0.008

well dark matter halo profiles in ΛCDM as in the other (coupled) dark energy models. While this is in contrast with the early findings of Macciò et al. (2004), it is however in good agreement with the subsequent works of Baldi et al. (2010) and Li & Barrow (2011b), who also found the NFW profile to be a valid description of DM haloes in interacting cosmologies. Thus, defining concentrations using Eq. (12) will not pose any problems nor introduce any systematic effect due to the fact that the NFW profile might only be valid for ΛCDM dark matter haloes.

In Fig. 3 we now show the median concentration for objects in a certain mass bin: cDE cosmologies have a smaller concentration than ΛCDM i.e. the larger the β the smaller the c; whereas the opposite is true for the uDE model. This can partly be explained by the fact that concentrations are related to the formation time of the halo, since structures that collapsed earlier tend to have a more compact centre due to the fact that it has more time to accrete matter from the outer parts. Dynamical dark energy cosmologies generically imply larger c values as a consequence of earlier structure formation, as found in works like those by Dolag et al. (2004), Bartelmann et al. (2006) and Grossi & Springel (2009). In fact, since the presence of early dark energy usually suppresses structure growth, in order to reproduce current observations we need to trigger an earlier start of the formation process, which on average yields a higher value for the halo concentrations. However, as explained in Baldi et al. (2010), smaller concentrations in cDE models are not related to the formation time of dark matter halos, but to the fact that one of the effects of coupled quintessence is to effectively act as a positive friction term. This means that dark matter particles have an increased kinetic energy, which moves the system out of virial equilibrium and causes a slight expansion, resulting in a lowering of the concentration.

In the hierarchical picture of structure formation, concentrations are usually inversely correlated to the halo mass as more massive objects form later; N-body simulations (Dolag et al. 2004; Muñoz-Cuartas et al. 2011; Prada et al. 2012) and observations (Comerford & Natarajan 2007; Okabe et al. 2010; Sereno & Zitrin 2012) have in fact shown that the relation between the two quantities can be written as a power law of the form

$$c(M) = c_0 \left(\frac{M_{200}}{10^{14} M_{\odot} h^{-1}} \right)^{\gamma} \qquad (13)$$

where γ and c_0 can have explicit parametrizations as functions of redshift and cosmology (see Neto et al. 2007; Muñoz-Cuartas et al. 2011; Prada et al. 2012). When we fit our halo sample to this relation using c_0 and γ as free parameters we obtain the best-fit values as shown in Table 5. Our values are qualitatively in good agreement with the ones found by, for instance, Macciò et al. (2008) and Muñoz-Cuartas et al. (2011) for ΛCDM; but we do find some tension with the findings of Prada et al. (2012). However, since they use a different algorithm for the determination of c (which, according to them, leads to higher concentration values) and a different σ_8 normalizations we cannot directly compare our results to theirs. On the other hand, uDE values are generally in agreement with Dolag et al. (2004), De Boni et al. (2013) although in both cases there are again some discrepancies in the c_0 best-fit result, most probably due to the much different σ_8 used in their simulations. For cDE we cannot directly compare our concentration-mass relation to the one obtained by Baldi et al. (2010) since they do not provide any fit to Eq. (13).

Table 6. Fraction of total dark matter mass for different node type in each simulation.

cell type	ΛCDM	cDE	cDE033	cDE066	cDE099
void	0.103	0.103	0.102	0.103	0.102
sheet	0.343	0.343	0.344	0.344	0.343
filament	0.437	0.438	0.443	0.442	0.443
knot	0.116	0.115	0.109	0.111	0.118

Table 7. Fraction of total gas mass for different node type in each simulation.

cell type	ΛCDM	cDE	cDE033	cDE066	cDE099
void	0.103	0.103	0.103	0.104	0.102
sheet	0.349	0.348	0.348	0.347	0.346
filament	0.449	0.450	0.450	0.449	0.453
knot	0.097	0.097	0.097	0.098	0.098

Table 8. Volume filling fractions of different cell types for all the simulation set.

cell type	ΛCDM	cDE	cDE033	cDE066	cDE099
void	0.337	0.338	0.338	0.337	0.334
sheet	0.460	0.456	0.460	0.460	0.461
filament	0.185	0.184	0.185	0.185	0.186
knot	0.017	0.017	0.017	0.017	0.018

5 PROPERTIES OF THE COSMIC WEB

We now turn to the study of the cosmic web, as defined in Section 3.3, in ΛCDM, uDE, cDE033, cDE066 and cDE099. In Fig. 4 and Fig. 5 we give a visual impression of the web classification (left) and the underlying dark matter density field (right) for a slice of thickness one cell (i.e. $0.97h^{-1}\,\mathrm{Mpc}$) using a logarithmic colouring scheme for the density. From Figs. 4 & 5 it is evident that there is, in general, a very close correspondence between $\delta > 1$ and filamentary and knot-like regions; just like between $\delta < 1$ and void and sheet-like ones, so that the kinetic classification does provide in general a faithful description of the underlying density distribution – as shown in Hoffman et al. (2012). Nonetheless, a minor number of cells do indeed violate this principle. In fact, as also noted by Hoffman et al. (2012), in a very limited number of cases it happens

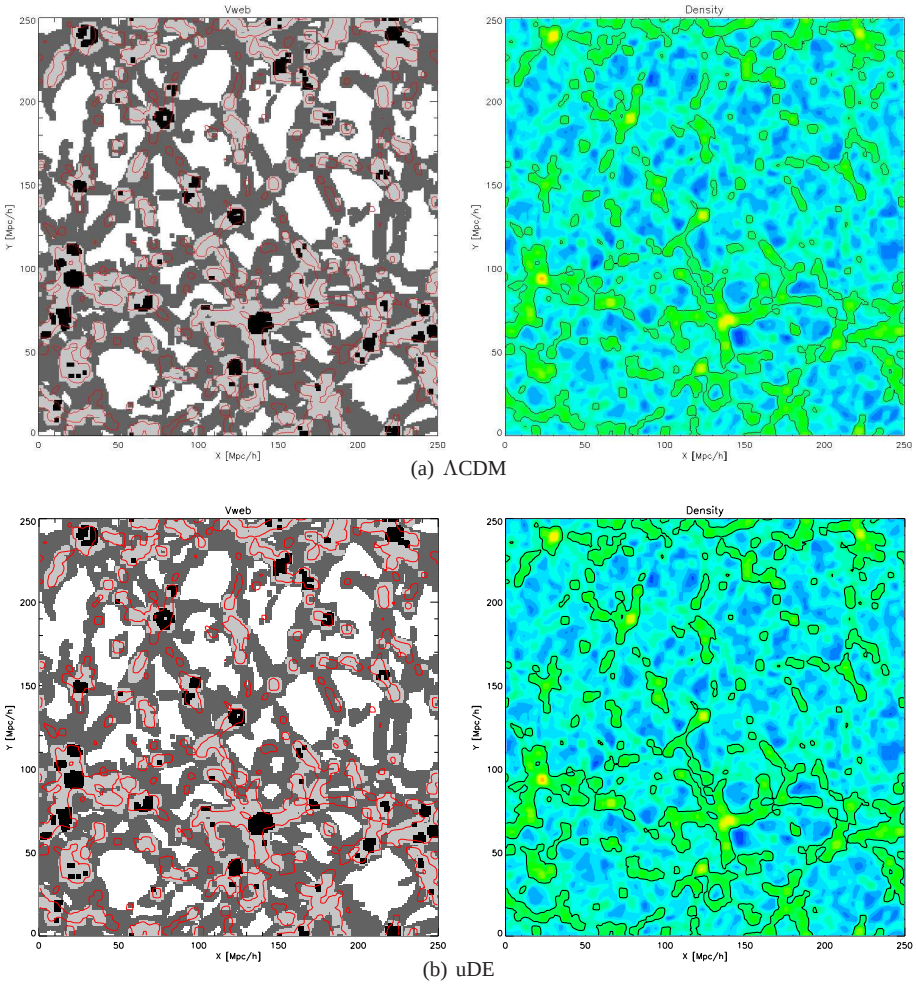

(a) ΛCDM

(b) uDE

Figure 4. Cosmic web and matter density field plots for ΛCDM (upper panel) and uDE(lower panel). In the left panels of each pair we plot voids (white points), sheets (dark grey), filaments (light grey) and knots (black), while on top of them we depict red contours enclosing the regions where $\delta > 1$. The right panel of each pair show the colour coded logarithmic matter density, the black solid contours again encompass overdense regions. We notice that there's a very good overlap of overdense regions with filaments and knots, while underdense ones can be identified with voids and sheets.

that, for cells placed in the interior of a of a large dark matter halo, the velocity field will be determined by the motion of its virialized particles and not reflecting the cosmic web, respectively. On top of that, we must not forget that the freedom in the choice of the threshold λ_{th}, and the fixed spacing of the grid account for the fact that on scales smaller than $0.97h^{-1}\,\mathrm{Mpc}$ we cannot properly resolve the complex shape of the web, which would probably require a more flexible grid implementation (Platen et al. 2011). However, all these shortcomings do not seriously invalidate this description, as the number of such cells is generally small (for example, points defined as voids with $\delta > 1$ sum up to less than 1% of the total in all simulation, and independent of the simulation). In fact, the latter is the most important condition that we need to ensure, so that the existence of small biases disappears when considering ratios to ΛCDM, which is at the core of the analysis we are carrying.

In Tabs. 6, 7 & 8 we show the mass and volume filling fractions as a function of cell type and cosmologies. These values are estimated simply summing all masses and volumes contained in cells belonging to the same kind of environment. What is clear by looking at these results is that the general structure of the cosmic web is almost left unchanged across models. In fact, discrepancies among different cosmologies are much less than 1% in this regard, thus making it hard to detect deviations from ΛCDM by simply considering the volume and the mass associated to the various kinds of environment. The same conclusion can be drawn if we look at Fig. 6, which shows the distributions of the three $\lambda_{1,2,3}$ eigenvalues of $\Sigma_{\alpha\beta}$, that appear to be identical and thus provide no leverage to distinguish the models under investigation here.

The gas distribution through the different node types seems also to be largely unaffected by the different cosmology: As we can see from Table 7, the mass fractions of gas are substantially identical throughout all the models, without any significant discrepancy. Comparing to the distribution of dark matter, we do notice a slight increase in the fraction of gas belonging to sheets and filaments paralleled by its reduction on knots, a pattern which is observable in all the models to the same extent.

We remark that our results for uDE agree with Bos et al. (2012), who also found that quintessence cosmologies with Ratra-Peebles potentials do not lead to significant changes in the general properties of the cosmic web. We also emphasize that our findings relative to void regions are largely independent of the choice of λ. Using different threshold values we have been able to test this and

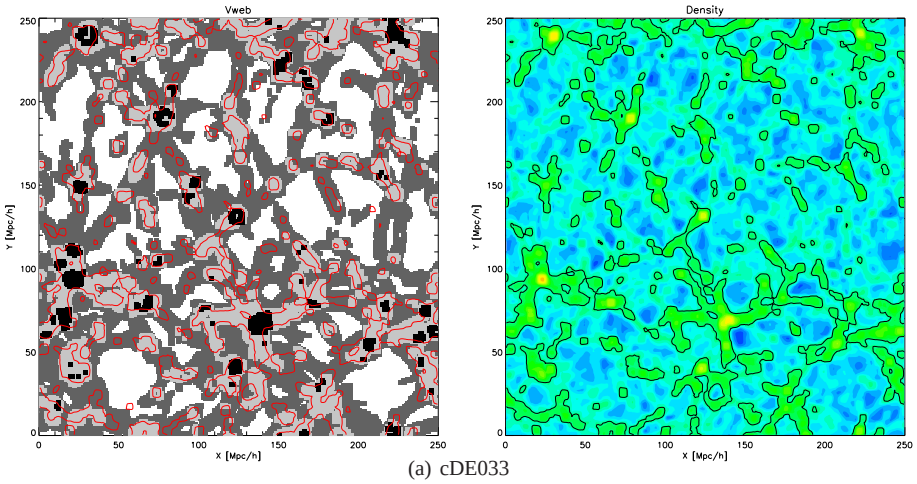

(a) cDE033

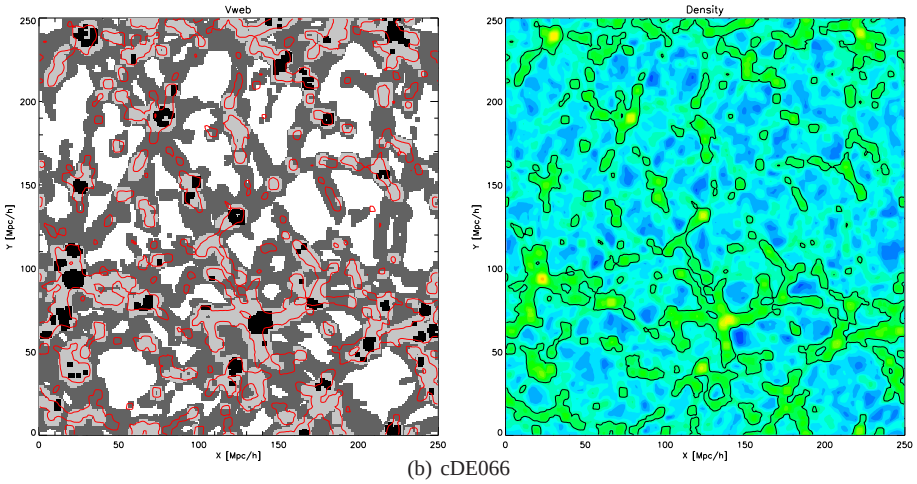

(b) cDE066

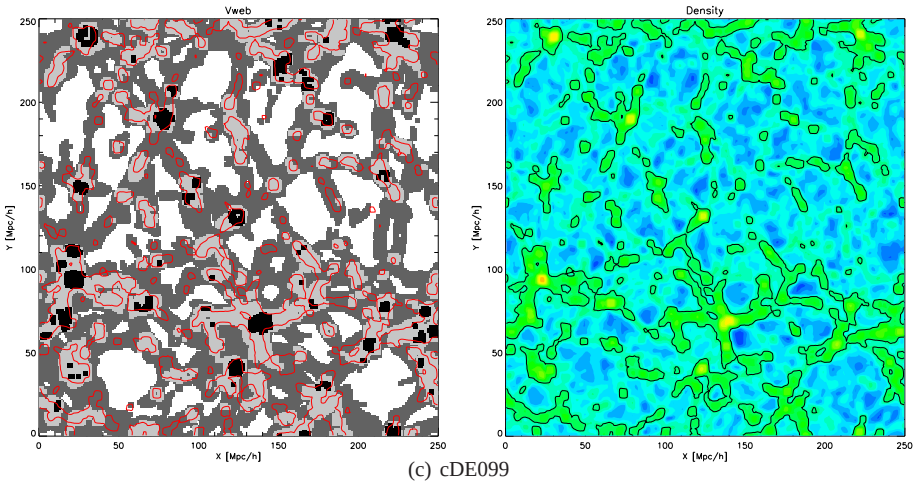

(c) cDE099

Figure 5. Same as Fig. 4 for cDE033 (upper panel), cDE066 (middle panel) and cDE099 (lower panel).

see that void distributions are affected to the same degree in all the different models, confirming this particular result does not depend on our λ_{th}.

6 HALO PROPERTIES IN DIFFERENT ENVIRONMENTS

We now turn to the study of halo properties classified according to their environment; this kind of analysis has already been done for ΛCDM using both geometrical (e.g. Avila-Reese et al. 2005; Macciò et al. 2007) and dynamical (e.g. Hahn et al. 2007;

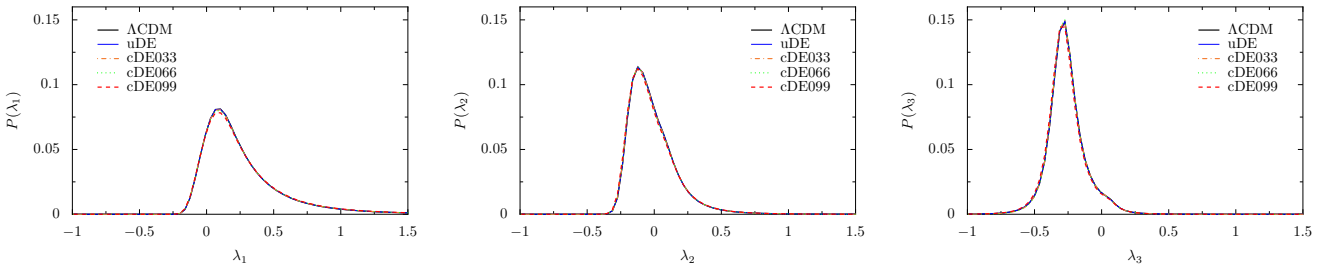

Figure 6. Probability distributions for the eigenvalues of the velocity shear tensor at all nodes. At every node we assume $\lambda_1 > \lambda_2 > \lambda_3$. The distributions are almost identical for all simulations and eigenvalues, except for a progressively lower peak of $P(\lambda_1$ (left panel) for coupled models.

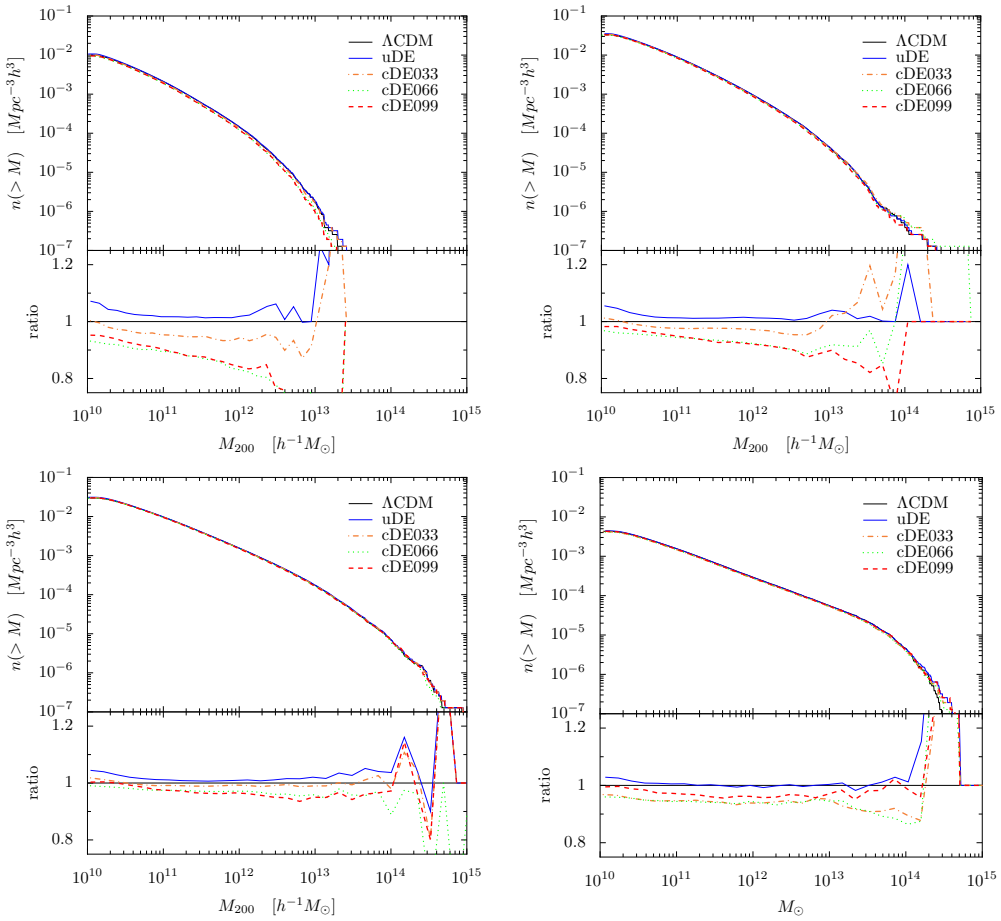

Figure 7. Upper panels: halo mass function in voids (left) and sheets (right). Lower panels: halo mass function in filaments (left) and knots (right).

Libeskind et al. 2012, 2013) web classifications, finding in general a correlation between halo properties such as spin and shape to its surrounding environment.

Using the information from the halo catalogues we proceed to assign each halo to the nearest grid point and build up four different halo samples, one for each cell type. Then we repeat the analysis presented in Section 4 for the halo counts (velocity and mass), spin and concentrations. We will see that this kind of separation of haloes enhances some of the differences already seen in general among different cosmological models and is therefore of great importance when trying to constrain more effectively coupled and uncoupled scalar field cosmologies.

Voids and sheets are readily identified with underdense regions, as has also been confirmed by the analysis presented in the previous Section 5. And the fact that for these cells at most one eigenvalue of the shear tensor has a value above λ_{th} means that in two or more spatial directions there is a net outflow of matter, which is in turn associated with a matter density below the average. For overdense regions (i.e. filaments and knots) there is a net inflow of matter towards the center of the cell from at least two directions. Following this we partition the subsequent study into underdense regions on the one hand (using voids and sheets) and overdense regions (i.e. filaments and knots) on the other.

Underdense regions in ΛCDM are usually associated with lower spins and slightly larger halo concentrations (Macciò et al.

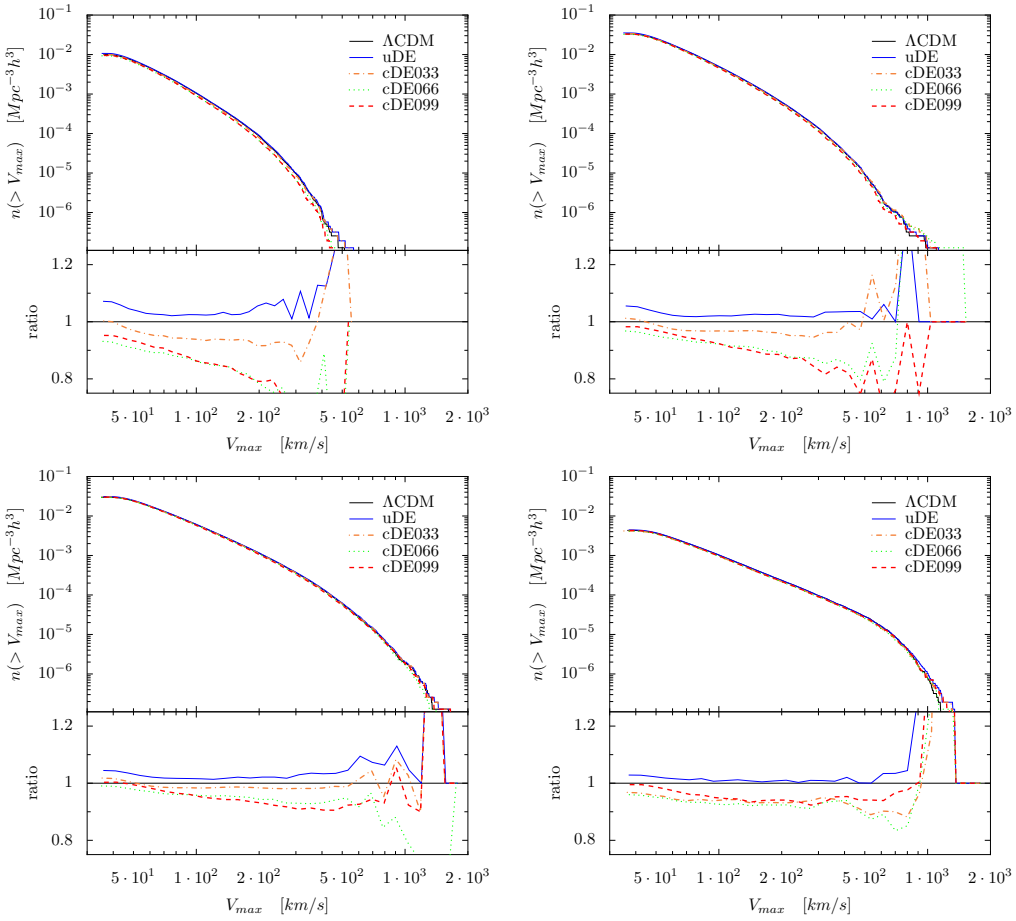

Figure 8. Upper panels: halo velocity function in voids (left) and sheets (right). Lower panels: halo velocity function in filaments (left) and knots (right).

Table 9. Fraction of haloes above $10^{10}h^{-1}\mathrm{M}_{\odot}$ per environment type, in each cosmological model.

Environment	ΛCDM	uDE	cDE033	cDE066	cDE099
void	0.128	0.131	0.127	0.123	0.124
sheet	0.431	0.432	0.431	0.429	0.428
filament	0.384	0.382	0.387	0.392	0.391
knot	0.055	0.054	0.053	0.055	0.056

2007), raising the question whether this still holds for (coupled) dark energy cosmologies.

6.1 Halo number counts

Even though, by definition, underdense regions are less populated, non-negligible fractions of the total halo count can be still found in voids and sheets, as shown in Table 9, ensuring that the samples used are reasonably large, and allow us to draw credible conclusions.

6.1.1 Underdense regions: voids and sheets

We notice that in underdense regions (i.e. voids and sheets, shown in the upper two plots) the trend persists that the number of objects is smaller for cDE models than for ΛCDM, something also observed for the general halo sample. However, it is important to remark that singling out and counting the objects belonging to the underdense parts only, we end up observing larger differences among the models. This effect also appears to be much stronger in cDE than in uDE. In fact, whereas the differences in number counts of objects does not exceed 7%, when restricting halo counts to void regions only, we can see that cDE models' underprediction is much larger and peaks at 20% (ignoring the higher mass ends, where only a small number of objects is found). It is also clear from Fig. 8 that while the sign of the effect is very similar in both voids and sheets, its strength is slightly reduced in the latter type of web, suggesting that there exists at least a mild dependence of this phenomenon on the specific kind of environment. Although we are not showing it here, we have also carefully checked that this result is substantially independent from the kind of λ_{th} chosen. In fact, repeating our computation using higher threshold values, we

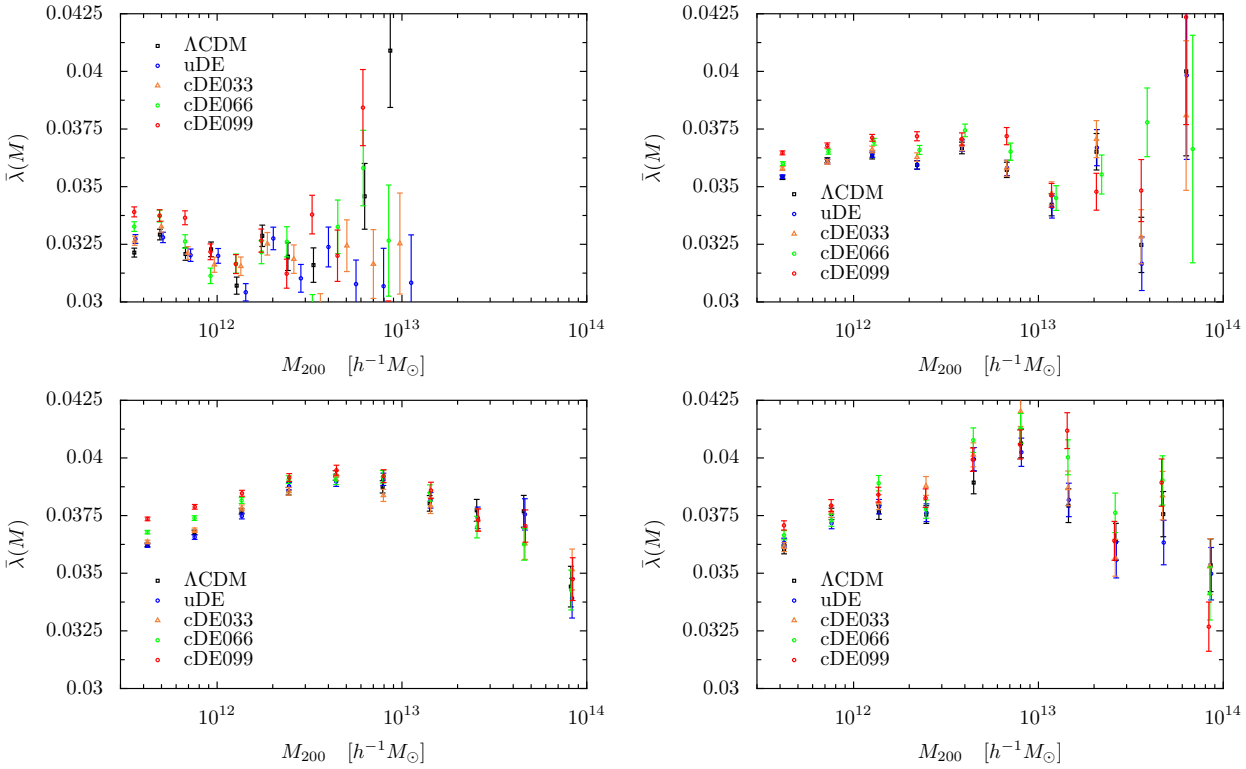

Figure 9. Median of the spin parameter for haloes located in voids (upper left panel), sheets (upper right panel) filaments (lower left panel) and knots (lower right panel).

see that the magnitude of the effect does not change substantially. The physical mechanism behind this effect is understood and provides a consistent framework for interpreting our results. In fact, as first explained by Keselman et al. (2010) and subsequently confirmed by Li & Barrow (2011b), fifth forces enhance the gravitational pull towards the overdense regions, quickly evacuating matter from underdense regions. This causes these environments to have less structures, so that in the end the number of haloes left in voids will be comparatively smaller than in the non-interacting cases, as found in our simulations.

However, we need to make an additional remark on this result before proceeding to the next section. In fact, we note that our choice of the σ_8 normalization, which is taken to be the same at $z = 0$, plays an important role in the result just described. It is in fact known (see e.g. Baldi & Pettorino 2011) that using a different normalization prescription (for instance, at the redshift of the CMB for the matter density fluctuations), coupled models end up predicting (in total) more objects than ΛCDM. Hence, at this stage we cannot completely disentangle the influence of our choice of the normalization of the initial conditions from the genuine influence of the additional interaction.

6.1.2 *Overdense regions: filaments and knots*

Like in the case of underdensities, we notice for overdense regions (shown in the lower two plots) that the trend of suppression which characterizes the general halo counting still holds, even though now the strength of this effect is slightly smaller across all cosmologies. This is not unexpected, since the effect seen in the HMF discussed in Section 4 has to be obtained from a combination of both underdense and overdense structures, and should therefore result in an intermediate value for cDE halo underproduction. Again, we have checked that the chosen threshold for the eigenvalues of the velocity shear tensor does not substantially affect this conclusion.

We can therefore state that there is a progression towards smoothing out the differences among different cosmologies while moving to increasingly higher density regions. *This is a very important result that indicates that underdense regions should be the target of choice when searching for the effects of additional long range gravitational-like forces.*

This result is in line with what has been already found for other fifth-force cosmologies (see Martino & Sheth 2009; Keselman et al. 2010; Li et al. 2012; Winther et al. 2012), where the environmental dependence and in particular the properties of voids were stressed as powerful tests for additional interactions and modifications of standard Newtonian gravity. It is in fact well known that void properties are extremely sensitive to cosmology (Lee & Park 2009; Lavaux & Wandelt 2010; Bos et al. 2012; Sutter et al. 2012) and hence provide a powerful probe of alternative models. In particular, when the extra coupling in the dark sector is weak (as in the cases analyzed here) the complex evolution and phenomena that characterize the overdense regions may conceal its imprints, while void regions, whose dynamics is comparatively simpler, are expected to be more directly linked to the underlying cosmology.

6.2 Spin and concentration

We now turn to the non-dimensional spin parameter, λ, and dark matter halo concentrations, investigating how they will change

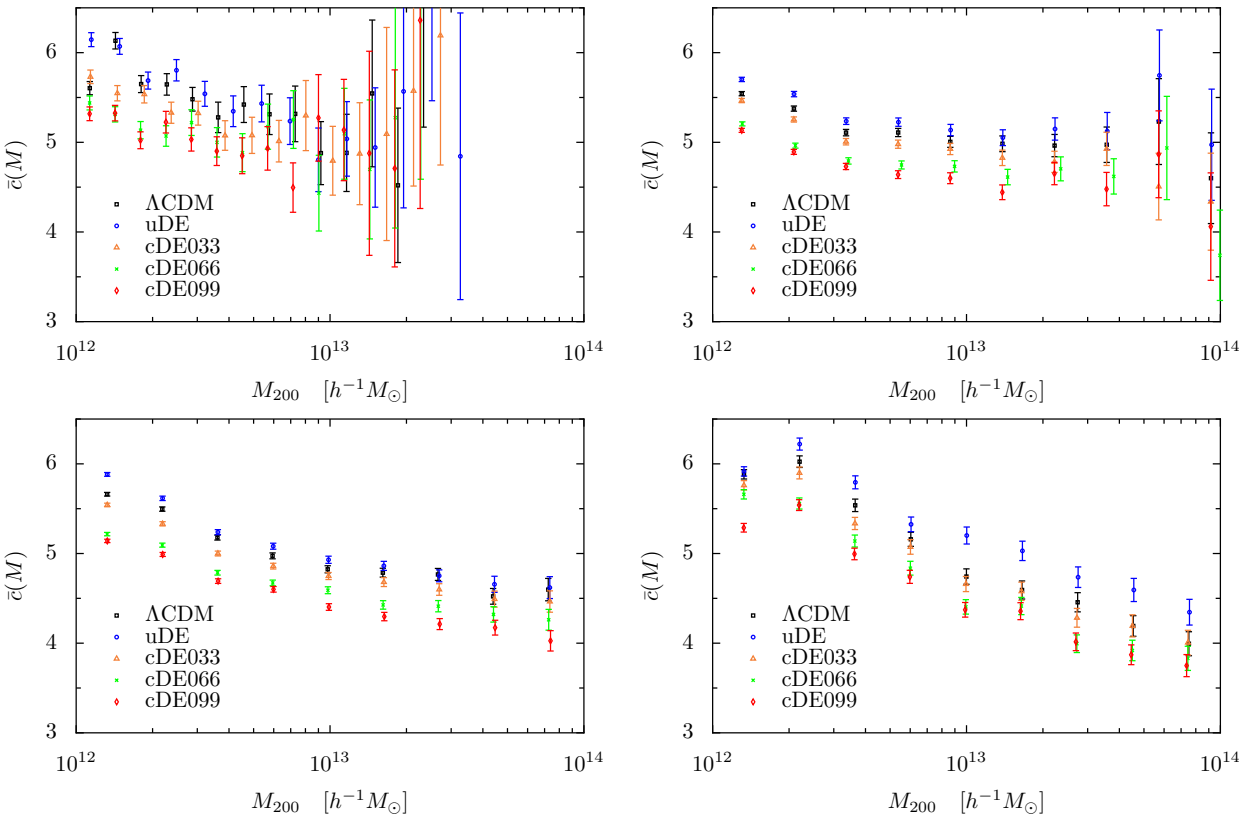

Figure 10. Average concentration for haloes located in voids (upper left panel), sheets (upper right panel), filaments (lower left panel) and knots (lower right panel).

Table 10. Best fit values for the concentration-mass Eq. (13) relation for haloes belonging to voids (v) sheets (s) filaments(f) and knots (k).

Parameter	ΛCDM	cDE	cDE033	cDE066	cDE099
c_0(v)	5.1 ± 0.5	5.36 ± 0.5	4.5 ± 0.2	4.5 ± 0.3	4.3 ± 0.3
γ(v)	-0.03 ± 0.01	-0.03 ± 0.01	-0.04 ± 0.01	-0.04 ± 0.01	-0.03 ± 0.01
c_0(s)	4.8 ± 0.1	5.1 ± 0.2	4.5 ± 0.1	4.3 ± 0.2	4.2 ± 0.1
γ(s)	-0.034 ± 0.007	-0.037 ± 0.009	-0.04 ± 0.01	-0.04 ± 0.01	-0.036 ± 0.008
c_0(f)	4.41 ± 0.05	4.42 ± 0.03	4.26 ± 0.05	4.15 ± 0.04	3.98 ± 0.05
γ(f)	-0.052 ± 0.01	-0.059 ± 0.006	-0.07 ± 0.01	-0.064 ± 0.008	-0.058 ± 0.005
c_0(k)	4.06 ± 0.07	4.38 ± 0.08	4.02 ± 0.06	3.74 ± 0.06	3.67 ± 0.07
γ(k)	-0.087 ± 0.009	-0.093 ± 0.008	-0.085 ± 0.005	-0.093 ± 0.009	-0.092 ± 0.007

across different environments and cosmologies. In the latter case, we will also pay particular attention to the environment-related changes to the $c - M$ relation of Eq. (13). In both cases we refer to the definitions introduced in Section 4.

6.2.1 Underdense regions: voids and sheets

Looking at the median spin parameters shown in the upper panel of Fig. 9 we can again draw the conclusion that, just like in the general case, cDE cosmologies lead to larger spins and that this increase is proportional to the coupling parameter β. On the other hand, the value of $\bar{\lambda}$ for haloes in uDE cosmologies is, on average, indistinguishable from ΛCDM. We can therefore confirm the observation that underdense region contain haloes with lower spins, just as found by Macciò et al. (2007). However, the reduction in the median value is of the same order in all models, so that combining the information of the environment does not put tight constraints on the parameters of the model.

Concentrations, too, show a remarkable behaviour for haloes belonging to underdense regions. In Table 10 we show the results of fitting the median concentration per mass bin to a power law, i.e. Eq. (13). The first thing we observe is that the correlation between c and M (as measured by the power-law index γ) is weaker than what we observed in the general case. This, combined with the fact that in the lower mass bins median concentration do not change with respect to the general case, in turn leads to observed larger values for c_0, although the errors are also large due to the small number statistics. However, some care must be taken when

considering this relation for void haloes since the fit is based upon a small mass range only and also gives more weight to lower mass objects (Prada et al. 2012; De Boni et al. 2013).

6.2.2 Overdense regions: filaments and knots

In the bottom panels of Fig. 9 and Fig. 10 we plot the spin and concentration-mass relation; the best-fit values to Eq. (13) are again provided in Table 10.

In the case of spins, we find that dark matter haloes in coupled cosmologies tend to be characterized by larger values of λ. However, haloes located in filamentary structures show, at least in the lower mass bins, sharper differences between cDE models and ΛCDM than what is revealed by knots. This is also due to the smaller number of low mass haloes living in knots, which visibly affects the statistics of the parameter.

Concentrations instead show two slightly different patterns in filaments and in knots. In the former environment, all cosmologies seem to be characterized by a flatter slope, which averages around -0.06 and seems not to be connected to the underlying model. In the latter environment, a steeper correlation is found, with $\gamma \approx -0.09$ – much closer to the general case discussed in Section 4. Not only the slope but also the normalization c_0 of Eq. (13) changes when considering filamentary or knot-like environments: in the former case we find that this parameter is substantially larger than in the latter.

Our results therefore indicate that the concentration-mass relation is not only affected by the cosmological model but also by the environment the haloes under consideration live in: γ gets flatter while c_0 increases for decreasing densities. However, at odds with what we found for halo number counts, we find here that environment does not play a role in strengthening the magnitude of model-dependent properties of haloes. While the effect of dark energy can still be clearly seen in the higher spins and lower concentrations of dark matter haloes, these cDE-induced characteristics are not enhanced by the environment. In fact, whereas the halo content of the different regions depends on the model and reinforces the trends observed in Section 4.2, the properties of the haloes themselves, while still being correlated to the underlying cosmology, seem to be shifted by the same amount as ΛCDM. This suggests that environmental effects, in these cases, influence to the same extent both quintessential and standard models, and do not provide a stronger model-specific kind of prediction.

7 CONCLUSIONS

In the present work – which forms part of a series of studies of (coupled) dark energy models – we have discussed the properties of large-scale structures and the cosmic web as they emerge in a series of different quintessence models, systematically comparing the results of a coupled scalar field to those obtained for a free field and the standard ΛCDM cosmology.

We performed the following three-fold analysis:

- we studied halo mass function and general halo properties (mass, spin and concentrations),
- we investigated the general properties of the cosmic web, using a kinetic classification algorithm,
- we correlated halo properties to the environment.

First, we have studied several aspects of cDE and uDE cosmologies looking at the full halo sample. At this stage, our results proved to be in line with those of Baldi et al. (2010); Li & Barrow (2011b); Cui et al. (2012), finding that the analytical formulae for the halo mass functions and dark matter profiles are valid also in this class of models.

Examining concentrations we found that, while uDE cosmology is characterized by haloes with higher values for c, for cDE models the opposite is in general the case – in accordance with the results of Baldi et al. (2010) and De Boni et al. (2013). Interestingly, in the case of spin parameters we observe a weak dependence on the coupling, since we can see that their value is mildly enhanced by larger values of β, as was also noted by Hellwing et al. (2011) in the context of other fifth force cosmological models.

The cosmic web investigated as part of this study is characterized by the eigenvalues of the velocity shear tensor, a novel method recently proposed by Hoffman et al. (2012) and successfully applied to various simulations by Libeskind et al. (2012). Computing the fraction of total mass and volume belonging to each type of environment in our cosmologies, we find that the structure of the cosmic web itself does not reveal any particular difference among the models. The same conclusion can be drawn when investigating the global distribution of the shear tensor eigenvalues.

This notwithstanding, the classification of the cosmic web can be extremely useful when married with the halo catalogue. Combining the two, in fact, we were able to show that many of the differences observed in some halo properties when studying a global sample of relaxed structures above a threshold mass are in fact due to objects belonging to a certain type of environment. This happens in particular in voids and sheets, where the differences among cDE and ΛCDM are up to three times as large as they are in the general case. We have been able to verify how the magnitude of this effect is closely dependent on the coupling: while cDE cosmologies' underproduction of haloes in these regions is largely amplified, the overproduction that characterizes the uDE model investigated here is only weakly enhanced. This means that;

- one should focus on voids and sheets (underdense regions) when looking for signatures of (coupled) dark energy, and
- the magnitude of the deviations from ΛCDM allows us to place constraints on cDE cosmologies, or even detect them.

We have also seen how the standard concentration-mass relation is substantially affected when fitted for halo samples classified according to the environment they are located in. While the standard functional form of Eq. (13) still holds in underdense regions for all the models, it does so with a much steeper slope (the change is from an average of -0.9 to -0.4) and a substantial increase in the average concentration. In addition to this, we note again an amplification of the difference between the c_0 values in cDE and ΛCDM obtained when fitting Eq. (13) in voids and sheets (up to 15%) with respect to the global one (≈ 7 per cent).

The fact that these results are mostly visible when restricting the halo sample to underdense environments tells us the importance of the relative weights to be attached when performing global analyses. Indeed, when referring to halo properties in general, we do in fact hide a large number of peculiar features which can be seen only in a narrower subset. In the particular case of cDE we have seen how structures in voids play a major role, in the same direction of Li & Barrow (2011b), who also highlighted the importance of underdense regions in the context of similar cosmological models.

As a concluding remark, we would like to emphasize that a great amount of effects observed here still deserve a more in-depth study. In particular, the analysis of the temporal evolution of halo

parameters, will shed more light on the mechanisms that result in the previously discussed differences at $z = 0$ and increase the observational features that can be used to constrain quintessence models. We shall turn to these in future contributions in this series.

ACKNOWLEDGEMENTS

EC is supported by the *Spanish Ministerio de Economía y Competitividad* (MINECO) under grant no. AYA2012-31101, and MultiDark Consolider project under grant CSD2009-00064. He further thanks Georg Robbers for providing an updated, non-public version of `CMBEASY`.

This work was undertaken as part of the Survey Simulation Pipeline (SSimPL: ssimpluniverse.tk) and GFL acknowledges support from ARC/DP 130100117

AK is supported by the *Spanish Ministerio de Ciencia e Innovación* (MICINN) in Spain through the Ramón y Cajal programme as well as the grants AYA 2009-13875-C03-02, CSD2009-00064, CAM S2009/ESP-1496 (from the ASTROMADRID network) and the *Ministerio de Economía y Competitividad* (MINECO) through grant AYA2012-31101. He further thanks Emily for reflect on rye.

GY acknowledges support from MINECO under research grants AYA2012-31101, FPA2012-34694, Consolider Ingenio SyeC CSD2007-0050 and from Comunidad de Madrid under ASTROMADRID project (S2009/ESP-1496).

The authors thankfully acknowledge the computer resources, technical expertise and assistance provided by the Red Española de Supercomputación.

We further acknowledge partial support from the European Union FP7 ITN INVISIBLES (Marie Curie Actions, PITN-GA-2011-289442).

All the simulations used in this work were performed in the Marenostrum supercomputer at Barcelona Supercomputing Center (BSC).

REFERENCES

Abazajian K. N., et al., 2009, ApJS, 182, 543
Abdalla E., Abramo L. R., de Souza J. C. C., 2010, Phys. Rev. D, 82, 023508
Amendola L., 2000, Phys. Rev. D, 62, 043511
Amendola L., Quercellini C., 2003, Phys. Rev. D, 68, 023514
Aragón-Calvo M. A., van de Weygaert R., Jones B. J. T., van der Hulst J. M., 2007, ApJ, 655, L5
Armendariz-Picon C., Mukhanov V., Steinhardt P. J., 2000, Phys. Rev. Lett., 85, 4438
Avila-Reese V., Colín P., Gottlöber S., Firmani C., Maulbetsch C., 2005, ApJ, 634, 51
Baldi M., Pettorino V., 2011, MNRAS, 412, L1
Baldi M., Pettorino V., Robbers G., Springel V., 2010, MNRAS, 403, 1684
Barnes J., Efstathiou G., 1987, ApJ, 319, 575
Bartelmann M., Doran M., Wetterich C., 2006, A&A, 454, 27
Beltrán Jiménez J., Maroto A. L., 2008, Phys. Rev. D, 78, 063005
Bett P., Eke V., Frenk C. S., Jenkins A., Helly J., Navarro J., 2007, MNRAS, 376, 215
Beutler F., Blake C., Colless M., Jones D. H., Staveley-Smith L., Campbell L., Parker Q., Saunders W., Watson F., 2011, MNRAS, 416, 3017
Bond J. R., Kofman L., Pogosyan D., 1996, Nature, 380, 603
Bos E. G. P., van de Weygaert R., Dolag K., Pettorino V., 2012, MNRAS, 426, 440
Bullock J. S., Dekel A., Kolatt T. S., Kravtsov A. V., Klypin A. A., Porciani C., Primack J. R., 2001, ApJ, 555, 240
Caldwell R. R., Dave R., Steinhardt P. J., 1998, Physical Review Letters, 80, 1582
Carlesi E., Knebe A., Yepes G., Gottlöber S., Jiménez J. B., Maroto A. L., 2011, MNRAS, 418, 2715
Carlesi E., Knebe A., Yepes G., Gottlöber S., Jiménez J. B., Maroto A. L., 2012, MNRAS, 424, 699
Chiba T., De Felice A., Tsujikawa S., 2013, Phys. Rev. D, 87, 083505
Cole S., Lacey C., 1996, MNRAS, 281, 716
Comerford J. M., Natarajan P., 2007, MNRAS, 379, 190
Copeland E. J., Liddle A. R., Wands D., 1998, Phys. Rev. D, 57, 4686
Cui W., Baldi M., Borgani S., 2012, MNRAS, 424, 993
De Boni C., Dolag K., Ettori S., Moscardini L., Pettorino V., Baccigalupi C., 2011, MNRAS, 415, 2758
De Boni C., Ettori S., Dolag K., Moscardini L., 2013, MNRAS, 428, 2921
Dolag K., Bartelmann M., Moscardini L., Perrotta F., Baccigalupi C., Meneghetti M., Tormen G., 2004, Modern Physics Letters A, 19, 1079
Doran M., 2005, JCAP, 10, 11
Forero-Romero J. E., Hoffman Y., Gottlöber S., Klypin A., Yepes G., 2009, MNRAS, 396, 1815
Gardner J. P., 2001, ApJ, 557, 616
Gill S. P. D., Knebe A., Gibson B. K., 2004, MNRAS, 351, 399
Grossi M., Springel V., 2009, MNRAS, 394, 1559
Hahn O., Carollo C. M., Porciani C., Dekel A., 2007, MNRAS, 381, 41
Hellwing W. A., Cautun M., Knebe A., Knollmann S., Juszkiewicz R., 2011, ArXiv e-prints
Hockney R. W., Eastwood J. W., 1988, Computer simulation using particles
Hoffman Y., Metuki O., Yepes G., Gottlöber S., Forero-Romero J. E., Libeskind N. I., Knebe A., 2012, MNRAS, 425, 2049
Huterer D., 2010, General Relativity and Gravitation, 42, 2177
Jasche J., Kitaura F. S., Li C., Enßlin T. A., 2010, MNRAS, 409, 355
Jenkins A., Frenk C. S., White S. D. M., Colberg J. M., Cole S., Evrard A. E., Couchman H. M. P., Yoshida N., 2001, MNRAS, 321, 372
Kamenshchik A., Moschella U., Pasquier V., 2001, Physics Letters B, 511, 265
Keselman J. A., Nusser A., Peebles P. J. E., 2010, Phys. Rev. D, 81, 063521
Kitaura F. S., Jasche J., Li C., Enßlin T. A., Metcalf R. B., Wandelt B. D., Lemson G., White S. D. M., 2009, MNRAS, 400, 183
Klypin A., Macciò A. V., Mainini R., Bonometto S. A., 2003, ApJ, 599, 31
Knebe A., et al., 2013, ArXiv e-prints
Knebe A., Knollmann S. R., Muldrew S. I., Pearce F. R., et al., 2011, MNRAS, 415, 2293
Knebe A., Power C., 2008, ArXiv:0801.4453
Knebe A., Power C., 2011, in Wozniak H., Hensler G., eds, EAS Publications Series Vol. 44 of EAS Publications Series, A correlation between spin parameter and dark matter halo mass. pp 53–56
Knollmann S. R., Knebe A., 2009, ApJS, 182, 608
Komatsu E., et al., 2011, ApJS, 192, 18

Larson D., et al., 2011, ApJS, 192, 16
Lavaux G., Wandelt B. D., 2010, Mon.Not.Roy.Astron.Soc., 403, 1392
Lee J., Park D., 2009, Astrophys.J., 696, L10
Li B., Barrow J. D., 2011a, Phys. Rev. D, 83, 024007
Li B., Barrow J. D., 2011b, MNRAS, 413, 262
Li B., Zhao G.-B., Koyama K., 2012, MNRAS, 421, 3481
Libeskind N. I., Hoffman Y., Knebe A., Steinmetz M., Gottlöber S., Metuki O., Yepes G., 2012, MNRAS, 421, L137
Libeskind N. I., Hoffman Y., Steinmetz M., Gottlöber S., Knebe A., Hess S., 2013, ApJ, 766, L15
Macciò A. V., Dutton A. A., van den Bosch F. C., 2008, MNRAS, 391, 1940
Macciò A. V., Dutton A. A., van den Bosch F. C., Moore B., Potter D., Stadel J., 2007, MNRAS, 378, 55
Macciò A. V., Quercellini C., Mainini R., Amendola L., Bonometto S. A., 2004, Phys. Rev. D, 69, 123516
Martino M. C., Sheth R. K., 2009
Massey R., et al., 2007, Nature, 445, 286
Monaghan J. J., 1992, ARA&A, 30, 543
Muñoz-Cuartas J. C., Macciò A. V., Gottlöber S., Dutton A. A., 2011, MNRAS, 411, 584
Navarro J. F., Frenk C. S., White S. D. M., 1996, ApJ, 462, 563
Neto A. F., et al., 2007, MNRAS, 381, 1450
Novikov D., Colombi S., Doré O., 2006, MNRAS, 366, 1201
Nusser A., Gubser S. S., Peebles P., 2005, Phys.Rev., D71, 083505
Okabe N., Takada M., Umetsu K., Futamase T., Smith G. P., 2010, PASJ, 62, 811
Onions J., Knebe A., Pearce F. R., Muldrew S. I., Lux H., Knollmann S. R., Ascasibar Y., Behroozi P., Elahi P., Han J., Maciejewski M., Merchán M. E., Neyrinck M., Ruiz A. N., Sgró M. A., Springel V., Tweed D., 2012, MNRAS, 423, 1200
Pace F., Waizmann J., Bartelmann M., 2010, MNRAS, 406, 1865
Perlmutter S., et al., 1999, ApJ, 517, 565
Pettorino V., 2013, Phys. Rev. D, 88, 063519
Pettorino V., Amendola L., Baccigalupi C., Quercellini C., 2012, Phys. Rev. D, 86, 103507
Platen E., van de Weygaert R., Jones B. J. T., Vegter G., Calvo M. A. A., 2011, MNRAS, 416, 2494
Power C., Knebe A., Knollmann S. R., 2012, MNRAS, 419, 1576
Prada F., Klypin A. A., Cuesta A. J., Betancort-Rijo J. E., Primack J., 2012, MNRAS, 423, 3018
Ratra B., Peebles P. J. E., 1988, Phys. Rev. D, 37, 3406
Riess A. G., et al., 1998, AJ, 116, 1009
Sereno M., Zitrin A., 2012, MNRAS, 419, 3280
Sherwin B. D., et al., 2011, Physical Review Letters, 107, 021302
Springel V., 2005, MNRAS, 364, 1105
Springel V., 2010, ARA&A, 48, 391
Springel V., Yoshida N., White S. D. M., 2001, NewA, 6, 79
Sutter P. M., Lavaux G., Wandelt B. D., Weinberg D. H., 2012, ApJ, 761, 187
Tinker J., Kravtsov A. V., Klypin A., Abazajian K., Warren M., Yepes G., Gottlöber S., Holz D. E., 2008, ApJ, 688, 709
Tsujikawa S., 2013, ArXiv e-prints
Wang P.-Y., Chen C.-W., Chen P., 2012, JCAP, 2, 16
Warren M. S., Quinn P. J., Salmon J. K., Zurek W. H., 1992, ApJ, 399, 405
Wetterich C., 1995, A&A, 301, 321
Winther H. A., Mota D. F., Li B., 2012, ApJ, 756, 166
Zel'dovich Y. B., 1970, A&A, 5, 84
Zlatev I., Wang L., Steinhardt P. J., 1999, Physical Review Letters, 82, 896

This paper has been typeset from a TEX/ LATEX file prepared by the author.